Complement protein C1q is a therapeutic target for neuropathic pain

Noosha Yousefpour
McGill University
Shannon Tansley
Department of Psychology, McGill University, Montreal, QC
Samantha Locke
McGill University, Montreal, QC
Behrang Sharif
McGill https://orcid.org/0000-0002-6451-2596
Marc Parisien
McGill University https://orcid.org/0000-0003-2924-5960
Haley Deamond
McGill University, Montreal, QC https://orcid.org/0000-0002-2900-246X
Vidhu Mathur
Annexon Biosciences
Ted Yednock
Annexon Biosciences
Jean-Sebastien Austin
McGill University
Valerie Bourassa
McGill University https://orcid.org/0000-0002-0689-2287
Chengyang Wang
McGill University
Valérie Cabana
McGill University
Calvin Wong
McGill University
Kevin Lister
McGill University
Manon St-Louis
McGill University
Yaisa Andrews-Zwilling
Annexon Biosciences
Philippe Séguéla

McGill University https://orcid.org/0000-0001-7537-4427
Jeffrey Mogil
McGill University https://orcid.org/0000-0003-1359-5720
Yves De Koninck
CERVO Brain Research Centre https://orcid.org/0000-0002-5779-9330
Luda Diatchenko
McGill University https://orcid.org/0000-0002-1350-6727
Arkady Khoutorsky
McGill University
Alfredo Ribeiro-da-Silva (alfredo.ribeirodasilva@mcgill.ca)
McGill University https://orcid.org/0000-0002-4125-0255

Article

Keywords: Neuropathic pain, spinal cord, structural plasticity, microglia, synapse pruning, disinhibition, complement system, C1q

Posted Date: November 15th, 2021

DOI: https://doi.org/10.21203/rs.3.rs-1016420/v1

TITLE:

Complement protein C1q is a therapeutic target for neuropathic pain

AUTHORS: Noosha Yousefpour[1,3], Shannon N. Tansley[3,4], Samantha Locke[1,3], Behrang Sharif[3,5,9], Marc Parisien[3,8], Haley Deamond[1,3], Vidhu Mathur[10], Ted Yednock[10], Jean Sebastien Austin[4], Valerie Bourassa[1,3], Chengyang Wang[5], Valérie C. Cabana[1], Calvin Wong[3,6], Kevin Lister[3,4], Manon St-Louis[1], Yaisa Andrews-Zwilling[10], Philippe Seguela[3,5], Jeffrey S. Mogil[3,4], Yves De Koninck[1,3,7], Luda Diatchenko[3,6], Arkady Khoutorsky[3,6], Alfredo Ribeiro-da-Silva[1,2,3,*]

AFFILIATIONS:

1. Dept. of Pharmacology and Therapeutics, McGill University, Montréal, QC, Canada
2. Dept. of Anatomy and Cell Biology, McGill University, Montréal, QC, Canada
3. Alan Edwards Centre for Research on Pain, McGill University, Montréal, QC, Canada
4. Dept. of Psychology and Anesthesia, McGill University, Montréal, QC, Canada
5. Montreal Neurological Institute, Dept. of Neurology and Neurosurgery, McGill University, Montréal, QC, Canada
6. Dept. of Anesthesia and Faculty of Dentistry, McGill University, Montréal, QC, Canada
7. Depts. of Psychiatry and Neuroscience, Laval University, CERVO Brain Research Centre Québec, Québec, QC, Canada
8. Faculty of Dentistry, McGill University, Montréal, QC, Canada
9. Department of Physiology, McGill University, Montréal, QC, Canada
10. Annexon Biosciences, South San Francisco, CA, USA

[*]**CORRESPONDING AUTHOR:** alfredo.ribeirodasilva@mcgill.ca

SUMMARY

Activation of spinal microglia following peripheral nerve injury is a central component of neuropathic pain pathology. While the contributions of microglia-mediated immune and neurotrophic signalling have been well-characterized, the phagocytic and synaptic pruning roles of microglia in neuropathic pain remain unknown. Here, we show that peripheral nerve injury induces engulfment of dorsal horn synapses by microglia, leading to a preferential loss of inhibitory synapses. This synapse removal is dependent on the microglial complement-mediated synapse pruning pathway, as mice deficient in complement C3 do not exhibit synapse elimination. Furthermore, pharmacological inhibition of the complement protein C1q prevents dorsal horn inhibitory synapse loss and attenuates neuropathic pain. Thus, these results demonstrate that the complement pathway promotes persistent pain hypersensitivity via microglia-mediated engulfment and loss of inhibitory synapses in the dorsal horn of the spinal cord, revealing C1q as a novel therapeutic target in neuropathic pain.

KEYWORDS

Neuropathic pain, spinal cord, structural plasticity, microglia, synapse pruning, disinhibition, complement system, C1q.

INTRODUCTION

Damage or disease of the nervous system can provoke a form of a pathological pain known as neuropathic pain [1]. Symptoms of this debilitating disorder include spontaneous, ongoing, or shooting pain, in addition to an amplified pain sensation in response to both noxious and innocuous stimuli [2]. It is becoming increasingly evident that activation of spinal microglia, the resident immune cells in the central nervous system, plays a crucial role in the development of neuropathic pain [3,4]. Following nerve injury, spinal microglia increase in number and undergo drastic morphological changes [5]. These changes are accompanied by an upregulation of genes associated with the reactive state of microglia, the production and release of potent immune mediators and neuromodulators, and an increase in phagocytotic activity [6-8]. Of these functions, far less is known about the role of microglial phagocytosis within the context of synapse pruning, and its implications in modulating spinal cord synaptic connectivity in neuropathic pain. This is particularly important because maladaptive structural changes in the dorsal horn, such as loss of inhibitory synapses, are likely key contributing factors to the chronic nature of neuropathic pain [9,10].

During development, microglia prune synapses by employing various phagocytic signalling pathways [11]. In early postnatal life, microglia use the classical complement pathway to identify and remove weak synapses in the visual system [12]. In this model, complement proteins C1q and C3-derived complement fragment C3b are localized to synapses that are then targeted for engulfment by microglia via complement receptor 3 (CR3) signaling. On the other hand, microglia use the fractalkine receptor, CX3CR1, to regulate dendritic spine formation on hippocampal neurons [13]. Signaling between CX3CR1, and its ligand, neuronal CX3CL1, results in the elimination of weak synapses. Interestingly, these pathways are reactivated in several neurological disorders in adults [14-16]. In animal models of neuropathic pain, microglial surface receptors CR3 and CX3CR1 are upregulated in the spinal cord, suggesting that

these pruning pathways might play a role in the pain pathology. [17,18]. However, whether they directly contribute to the sensory symptoms of neuropathic pain remains unknown.

Here, we used a preclinical model of neuropathic pain to investigate engulfment of synaptic elements in combination with changes in synapse numbers in the dorsal spinal cord. We demonstrated that while nerve injury-activated microglia engulf both spinal inhibitory and excitatory terminals, there is a marked loss of inhibitory, but not excitatory synapses. Furthermore, we found that global depletion of microglia, genetic deletion of complement C3, and pharmacological inhibition of C1q fully protect against inhibitory synapse loss and unmask the dynamics of excitatory synapse changes. Therefore, we conclude that the complement pathway mediates synapse elimination in the dorsal horn of the spinal cord following nerve injury. Importantly, pharmacological inhibition of C1q alleviated mechanical hypersensitivity and interfered with the maintenance of the pathology. Together, these results uncover a previously unrecognized role of the CR3 synapse pruning pathway in neuropathic pain and reveal that targeting C1q is a novel disease-modifying strategy to prevent maladaptive dorsal horn synaptic reorganization following peripheral nerve injury.

RESULTS

Nerve injury triggers engulfment of presynaptic terminals by microglia

We first assessed the phagocytic capacity of spinal microglia to engulf inhibitory and excitatory neuronal elements at different time points after peripheral nerve injury. Mice were subjected to spared nerve injury (SNI), and engulfment of neuronal elements by dorsal horn microglia was quantified at day 3, 7, 14, and 21 post-SNI. To identify and differentiate inhibitory and excitatory neuronal structures, we used mice expressing TdTomato fluorescent protein in all inhibitory neurons ($Gad2^{Cre}$; tdTomato, referred to as Gad2-tdTom, Figure 1a) and substance P^{+} excitatory neurons ($Tac1^{Cre}$; tdTomato, referred to as Tac1-tdTom, Figure 1b). Substance P is expressed in a subset of excitatory spinal interneurons that are

implicated in nociceptive transmission [19]. We focused our analysis on lamina II of the spinal dorsal horn where neuronal circuits that are critical for sensory information processing exist [20]. To quantify engulfment of genetically labeled inhibitory and excitatory neuronal elements, high-resolution three-dimensional stacks of dorsal horn microglia were analyzed for the presence of neural-derived tdTomato$^+$ elements within microglial CD68$^+$ lysosomes (Figures 1c-d and S1a-b). Notably, a significant increase in the total volume of inhibitory and excitatory neuronal elements within lysosomes of ipsilateral microglia was observed at day 7 post-SNI, but not at day 3 (Gad2-tdTom: $t_{88} = 9.6$, $p < 0.0001$; Tac1-tdTom: $t_{88} = 7.4$, $p < 0.0001$) (Figures 1e and 1f). This phagocytic activity of microglia peaked at 7 days after injury and remained elevated for the following two weeks (Gad2-tdTom: $t_{88} = 3.7$, $P = 0.0012$; Tac1-tdTom: $t_{88} = 3.3$, $p = 0.0043$). Temporal analysis showed no significant difference in the time course of engulfment of inhibitory and excitatory elements, however, a greater volume of inhibitory as compared to excitatory elements was engulfed at day 7 post-SNI ($t_{22} = 1.3$, $P < 0.0001$) (Figure 1e and 1f).

To further study which sub-cellular components of dorsal horn neurons were engulfed by microglia, we performed immuno-colocalization analyses of CD68, and markers of different neuronal compartments within Iba1-labeled microglia. To assess the engulfment of synaptic terminals of inhibitory and excitatory interneurons, we used immunohistochemistry to detect synapse-specific proteins, VGAT and VGLUT2, respectively (Figures 1g and 1h). Engulfment quantifications of specific synaptic markers showed a similar trend to engulfment of neuronal elements (Figure 1i-j). At day 7 post-injury, there was a two-fold increase in the total volume of VGAT$^+$ and VGLUT2$^+$ terminals within microglial lysosomes sampled from the ipsilateral dorsal horn as compared to the contralateral side (VGAT: $t_{88} = 8.5$, $P < 0.0001$; VGLUT2: $t_{88} = 4.7$, $P < 0.0001$) (Figures 1i and 1j). Consistent with our previous results, we detected an increase in engulfment at day 14 and day 21 post-SNI for both synaptic markers (Figures 1i and 1j).

To determine whether other neuronal structures were engulfed by microglia, we examined the engulfment of neuronal cell bodies, marked by NeuN, as well as inhibitory (gephyrin) and excitatory

(homer1) postsynaptic structures and found no evidence of their engulfment at 3, 7, 14, and 21 days post-SNI (Figures S2a-c). We further counted dorsal horn inhibitory ($Gad2^+$) and excitatory ($Tac1^+$) neurons at day 21 post-injury and found no change in the number of these neurons suggesting that the increase in engulfment of presynaptic elements was not caused by neuronal loss (Figure S2d). Thus, both inhibitory and excitatory presynaptic terminals are engulfed by nerve injury-activated microglia in the dorsal horn of neuropathic mice.

Transient depletion of microglia attenuates mechanical hypersensitivity and prevents dorsal horn synapse loss

It is well established that microglia play an important role in neuropathic pain pathology [21] as both chronic or acute targeting of microglia have been shown to prevent and reverse pain behavior in models of neuropathic pain [4,7]. To study the contribution of microglia-mediated synaptic engulfment to neuropathic pain, we transiently depleted microglia during the peak of their engulfment activity, determined based on the temporal analysis of synapse engulfment (Figures 1i-j). To this end, we pharmacologically blocked microglial survival signaling, using PLX3397 (colony stimulating factor 1 inhibitor), for 6 consecutive days starting from day 5 post-injury (Figure 2a). PLX3397 depleted 91% of dorsal horn microglia and eliminated the nerve injury-induced difference in microglial count between ipsilateral and contralateral dorsal horn by the end of the treatment period on day 10 post-SNI (vehicle: $t_{40} = 9.2$, $P < 0.0001$; PLX3397: $t_{40} = 0.2$, $P > 0.9999$) (Figures 2b-c). Within 10 days following the end of treatment, microglia repopulated the dorsal horn with a greater number of cells in the ipsilateral side as compared to the contralateral side (vehicle: $t_{40} = 8.9$, $P < 0.0001$; PLX3397: $t_{40} = 3.6$, $P = 0.0026$) (Figures 2b and 2c). Next, we assessed the effect of transient depletion of microglia on mouse pain behavior. We observed a reduction in mechanical hypersensitivity at all time points following SNI in PLX3397-treated mice as compared to vehicle-treated mice (treatment × repeated measures: $F_{3,120} = 25.8$,

$p < 0.0001$) (Figure 2d). Importantly, the effect of transient depletion of microglia during the peak of engulfment persisted longer than the treatment period, suggesting that microglia-mediated synapse engulfment has a long-lasting effect on pain behaviour.

To determine whether nerve injury induces synapse loss and if this loss is caused by microglia-mediated engulfment of presynaptic terminals, dorsal horn inhibitory and excitatory synapse densities were quantified in neuropathic mice using structured illumination microscopy (SIM). For inhibitory synapses, presynaptic terminals were labeled with antibodies against VGAT, and postsynaptic sites were labeled with anti-gephyrin. A synapse was counted when VGAT and gephyrin immunoreactive puncta were in close apposition (Figure 2e). Consistent with previous reports [10], peripheral nerve injury resulted in a 27% reduction in the number of lamina II inhibitory synapses quantified as density of VGAT and gephyrin pairs (vehicle: $t_{96} = 4.0$, $P = 0.0002$) (Figure 2f). Notably, depletion of microglia prevented loss of inhibitory synapses in the ipsilateral dorsal horn without affecting the contralateral dorsal horn synapse density (PLX3397: $t_{96} = 0.3$, $P > 0.9999$) (Figure 2f). To assess excitatory synapse density, presynaptic terminals were labeled with anti-VGLUT2 antibody and postsynaptic excitatory sites were labeled with anti-homer1 antibody (Figure 2g). In lamina II of the dorsal horn, VGLUT2 marks terminals of IB4-binding peripheral sensory neurons as well as those of spinal cord excitatory interneurons. To exclude $VGLUT2^+$ terminals of sensory neurons from our analysis, we only quantified pairs between $VGLUT2^+$ terminals and $homer1^+$ postsynaptic puncta that were IB4 negative (Figure S3). Quantifications of $VGLUT2^+$ $IB4^-$ excitatory synapses showed no difference between ipsilateral and contralateral dorsal horns in vehicle-treated animals (vehicle: $t_{96} = 0.3$, $P > 0.99$) (Figure 2h). Surprisingly, microglial depletion resulted in a 13% increase in ipsilateral dorsal horn excitatory synapse density (PLX3397: $t_{96} = 2.5$, $P = 0.0232$) (Figure 2h). Taken together, these data show that transient depletion of microglia during the peak of synapse pruning attenuates mechanical hypersensitivity and prevents loss of dorsal horn inhibitory synapses in the SNI model of neuropathic pain.

Peripheral nerve injury induces microglial CR3 and CX3CR1-mediated synapse pruning pathways

We next investigated which microglial synapse pruning pathway mediates elimination of presynaptic terminals in neuropathic pain. RNA-seq data of spinal cord at day 7 post-SNI, when microglial engulfment activity peaks, was analyzed using selected Gene Ontology (GO) annotations and revealed that synapse pruning pathways were significantly up-regulated in the spinal cord of SNI mice as compared to naive animals (ES = +0.99, P = $1.0x10^{-2}$, FDR = 11%) [22]. Specifically, genes related to CR3 and fractalkine receptor (CX3CR1) pathways, two main molecular pathways associated with synapse pruning, were significantly increased (Figure 3a). We next assessed protein levels of the main signaling molecules within these pathways in the spinal cord of neuropathic mice.

In the CR3 synapse pruning pathway, C1q and C3-derived complement fragment C3b are localized to vulnerable synapses, promoting microglia-mediated synaptic engulfment via microglial C3 receptor (CR3) (Figure 3b) [12]. Quantification of C1q, and C3 protein levels in the dorsal horn of neuropathic mice at day 7 post-SNI revealed a significant increase in C1q and C3 expression (C1q: $t_9 = 17.9$, $P < 0.0001$; C3: $t_9 = 5.6$, $P = 0.0003$) (Figures 3c1-2, and 3d1-2). Moreover, the number of CR3 immunoreactive microglia was also significantly increased (≈ 3.5-fold) in the ipsilateral dorsal horn at day 7 post-injury (CR3: $t_7 = 11.7$, $P < 0.0001$) (Figures 3e1-2). Temporal analysis of C1q, C3, and CR3 expression showed an earlier and greater increase in CR3 and C1q levels starting at day 3 following injury (Figure S4a). This was followed by a significant increase of C3 at day 7 post-injury (D3 vs. D7: $t_{10} = 2.8$, $P = 0.0171$). By the end of the third week after injury, C1q expression showed a modest decline while C3 and CR3 levels remained stable (D7 vs. D21: $t_{10} = 2.4$, $P = 0.0356$) (Figure S4a).

The other major synapse pruning pathway identified in our RNA-seq dataset operates through the binding of the neuronal chemokine fractalkine (CX3CL1) to its microglial receptor CX3CR1 (Figure 3b) [13]. We

observed immunoreactivity of CX3CL1 in the dorsal horn of the spinal cord, however, further analysis of CX3CL1 expression showed no injury-dependent overall change (Figures 3f1-2). Conversely, there was a significant increase in CX3CR1 expression at 7 days post-injury, quantified as overall fluorescence intensity within the dorsal horn ($t_5 = 3.6$, $P = 0.0146$) (Figures 3g1-2) as well as per individual microglia cell ($t_{20} = 3.4$, $P = 0.0026$) (Figures 3h1-2). Temporal analysis of CX3CR1 expression after injury revealed a stable increase, starting on day 3, which persisted for three weeks after injury (Figure S4b). Taken together, these experiments provide evidence for the upregulation of CR3 and CX3CR1 synapse pruning pathways in the SNI model of neuropathic pain.

Nerve injury-induced engulfment of spinal presynaptic terminals is mediated by the CR3 pathway

Nerve injury-induced increases of CR3 and CX3CR1 pruning pathway components suggest that these pathways might be involved in synapse pruning in the spinal cord. To assess the respective contribution of the CR3 and CX3CR1 pathways to spinal cord synapse removal in neuropathic pain, levels of engulfment of inhibitory and excitatory presynaptic terminals were measured at the peak of synapse engulfment (i.e., 7 days after SNI) in mice lacking complement factor C3 (C3 KO) or CX3CR1 (CX3CR1 KO). In both KO mouse lines, peripheral nerve injury induced microgliosis (C3 KO: $t_{30} = 8.7$, $P < 0.0001$; CX3CR1 KO: $t_{30} = 6.0$, $P < 0.0001$) (Figures S5a-b) and a significant increase in the volume of $CD68^+$ lysosomal compartments in the ipsilateral dorsal horn (C3 KO: $t_{30} = 4.2$, $P= 0.0006$; CX3CR1 KO: $t_{30} = 3.1$, $P = 0.0104$) (Figures S5a and c). Although the increase in the number of microglia and lysosomal volumes in CX3CR1 KO mice was smaller as compared to C3 KOs and wildtype littermates (Figures S5a-c), engulfed inhibitory and excitatory terminals were still detected within CX3CR1 KO lysosomes in the ipsilateral dorsal horn (Figures 4a and 4c).

Quantifications of the total volume of $VGAT^+$ inhibitory terminals within microglial lysosomes showed a similar increase in microglia sampled from the ipsilateral dorsal horn of CX3CR1 KOs and wildtype

mice as compared to the contralateral side (Figures 4a-b). Significant engulfment of VGLUT2^{+} excitatory terminals was also detected in CX3CR1 KO mice but was less pronounced compared to wildtype mice (t_{42} = 4.2, P = 0.0024) (Figures 4c-d). Notably, C3 KO mice showed no engulfment of inhibitory and excitatory presynaptic terminals as demonstrated by significant reductions in the total volume of VGAT and VGLUT2 immunoreactive puncta within microglial lysosomes (Figures 4b and 4d). Therefore, these results indicate that the CR3 signaling pathway, but not the CX3CR1 pathway, is essential for increased engulfment of terminals by microglia in the SNI model of neuropathic pain.

We next evaluated the role of CR3 and CX3CR1 pruning pathways in remodeling dorsal horn synaptic connectivity in the SNI model of neuropathic pain. To this end, we quantified inhibitory and excitatory synapse densities in C3 KO and CX3CR1 KO mice 21 days after injury. Similar to wildtype mice, we found a 21% decrease in ipsilateral inhibitory synapse density (i.e., VGAT puncta juxtaposed gephyrin puncta) in CX3CR1 KO mice as compared to the contralateral side (CX3CR1 KO: t_{42} = 3.3, P = 0.0048) (Figures 4e-f). In contrast, a decrease in ipsilateral dorsal horn inhibitory synapses was prevented in C3 KO mice (Figures 4e-f). Quantification of excitatory synapses showed no change in VGLUT2^{+} excitatory synapse density in CX3CR1 KO mice as compared to wildtype animals (Figures 4g-h). However, ipsilateral dorsal horn VGLUT2^{+} excitatory synapse density in C3 KOs was increased by 9% as compared to the contralateral side (t_{42} = 4.2, P = 0.0104) (Figure 4h). Interestingly, a comparison of contralateral dorsal horn synapse densities revealed that C3 KO mice had a 20% increase in inhibitory synapse density and 24% increase in excitatory synapse density as compared to wildtype littermate controls, indicating a potential developmental deficit in refinement of dorsal horn synaptic connections (Figures 4f and 4h). Taken together, these data implicate the CR3 synapse pruning pathway, but not the CX3CR1 pathway, as the mechanism that modulates dorsal horn synaptic connectivity in the SNI model of neuropathic pain.

Complement protein C1q is expressed by nerve injury-activated microglia and localized to dorsal horn synapses

Complement protein C1q is the initiating factor of the classical complement cascade and has been implicated in the selective elimination or "pruning" of synapses through the CR3 pathway [12]. C1q levels are normally low in the adult CNS; however, normal aging, injury or certain diseases increase C1q expression [15,23,24]. Previous work in the CNS has revealed that both neurons and glia are capable of synthesizing C1q [25,26]. To determine whether neurons are the source of C1q in neuropathic pain, we performed fluorescent *in situ* hybridization for *C1qa* mRNA on spinal cord sections of Gad2-tdTom and Tac1-tdTom mice collected 7 days post-injury (Figure 5a). Consistent with the RNA-seq data, *C1qa* mRNA was upregulated (≈ 8-fold) as assessed by the number of *C1qa* mRNA immunoreactive puncta per $DAPI^+$ dorsal horn cell nuclei ($t_8 = 11.2$, $P < 0.0001$) (Figures 5a-b). Interestingly, the *C1qa* mRNA signal was almost completely excluded from $Gad2^+$ and $Tac1^+$ cell bodies, suggesting that these cells are not the source of *C1qa* (Figures 5a and c). We next closely examined the expression pattern of C1q protein in the dorsal horn of neuropathic mice. We observed strong and distinct C1q immunoreactivity localized within microglia that was significantly elevated in the ipsilateral dorsal horn ($t_{10} = 6.3$, $P < 0.0001$) (Figures 5d-e). In addition to the marked increase of C1q protein within microglia, a relatively smaller, punctate signal was scattered outside of microglia, and was only found in the ipsilateral dorsal horn (Figure 5d). To test if this extracellular C1q signal was associated with synaptic structures, we performed SIM on spinal cord sections immunolabeled for C1q as well as presynaptic markers for inhibitory ($VGAT^+$) and excitatory ($VGLUT2^+$) synapses. Consistent with our prediction, most extracellular C1q signals were in close proximity to presynaptic markers (Figure 5f). Quantification of the number of synapses in close proximity to C1q revealed a higher percentage of both inhibitory and excitatory synapses tagged with C1q in the ipsilateral dorsal horn as compared to the contralateral side (VGAT: $t_{36} = 12.4$, $P < 0.0001$; VGLUT2: $t_{36} = 3.5$, $P = 0.0024$) (Figure 5g). Interestingly, a larger

proportion of inhibitory synapses was marked by C1q as compared to excitatory synapses ($t_{18} = 9.1$, $P < 0.0001$) (Figure 5g). To determine whether the C1q deposited on synapses is secreted by microglia, we chronically depleted microglia using PLX3397 and assessed C1q protein expression in the dorsal horn at day 7 post-injury. Depletion of microglia resulted in almost complete elimination of C1q immunoreactivity in the dorsal horn, including C1q depositions on synapses (Figures 5h-j).

After establishing that C1q is released from nerve injury-activated microglia and deposited on synapses, we investigated whether expression of the apoptotic protein, cleaved caspase-3 (CC3), contributed to the recruitment of C1q to vulnerable synapses [27]. To answer this question, we analyzed inhibitory and excitatory presynaptic terminals for the presence of CC3 and C1q. Co-localization analysis showed that CC3 signal was rarely found at presynaptic terminals, and this was independent of C1q deposition at the synaptic site (Figures S6a-c). This indicates that CC3 does not drive injury-induced synapse pruning in the spinal cord. Together, these results demonstrate that C1q protein is produced by microglia and preferentially marks dorsal horn inhibitory synapses for elimination in the SNI model of neuropathic pain.

Inhibiting C1q attenuates neuropathic pain and protects dorsal horn synaptic circuitry

To determine whether induction of C1q expression in response to peripheral nerve injury causes synaptic reorganization in the spinal dorsal horn, we pharmacologically blocked C1q using anti-C1q antibodies (ANX M1.21). Anti-C1q antibodies were administered intraperitoneally every 4 days, starting 24 hours before SNI surgery. Mechanical hypersensitivity associated with neuropathic pain was assessed weekly (Figure 6A). Mice in both control (IgG isotope) and drug-treated groups developed mechanical hypersensitivity as shown by decreases in withdrawal thresholds of the ipsilateral hind paw (Figure 6B). Notably, at day 21 after injury, unlike IgG-isotope control-treated mice, both male and female ANX M1.21-treated animals showed a significant reduction in mechanical hypersensitivity ($t_{152} = 13.2$, $P =$

0.0065) (Figure 6b). Furthermore, SIM revealed a marked decrease in the number of ipsilateral C1q-associated inhibitory synapses in ANX M1.21-treated groups as compared to IgG-isotope control-treated mice ($t_{20} = 7.3$, $P < 0.0001$) (Figures 6c-d).

To study whether the effect of ANX M1.21 on neuropathic pain behavior was associated with disruption of the CR3 microglia-mediated synapse pruning pathway, we quantified engulfment of inhibitory and excitatory terminals by microglia in control and drug-treated animals. In line with our prediction, there was a significant reduction in inhibitory and excitatory presynaptic elements within ipsilateral microglial lysosomes of ANX M1.21-treated mice comparing to controls (inhibitory synapse engulfment: $t_{36} = 12.7$, $P < 0.0001$; excitatory synapse engulfment: $t_{36} = 2.8$, $P = 0.0136$) (Figures 6e-h). To test whether blocking C1q protects against nerve injury-induced synapse loss, we conducted synapse quantification in the dorsal horn of ANX M1.21 and IgG control mice 21 days after injury. ANX M1.21 prevented inhibitory synapse loss in the spinal dorsal horn (Figure 6i-l), resulting in a similar protective effect as observed with PLX3397 treatment and in C3 KO mice (ipsilateral inhibitory synapses: $t_{76} = 5.8$, $P < 0.0001$; ipsilateral excitatory synapses: $t_{76} = 5.2$, $P < 0.0001$). Altogether, these results demonstrate that targeting C1q, the initiating signaling protein of the CR3 synapse pruning pathway, protects the dorsal horn synaptic network and attenuates chronic neuropathic pain by inhibiting microglia-mediated synapse engulfment.

DISCUSSION

We have identified a novel mechanism by which microglia contribute to neuropathic pain through reorganization of the synaptic network in the spinal dorsal horn. We show that following peripheral nerve injury, activated microglia engage the classical complement pathway to remove spinal synapses. This is accomplished via the production and release of complement protein C1q, which is deposited on spinal synapses to tag them for removal through microglial C3R signaling. Pharmacological inhibition of C1q

protected spinal cord circuitry and prevented inhibitory synapse loss by disrupting synapse engulfment, thereby ameliorating neuropathic pain. These data implicate the C3R synapse pruning pathway as a major driver of structural synaptic plasticity in neuropathic pain and identify a novel therapeutic strategy to prevent the maintenance of the pain hypersensitivity.

Activation of spinal CR3 synapse pruning pathway in neuropathic pain

It is well established that microglia-mediated synapse pruning plays a key role in sculpting a functional neural network within the developing central nervous system [11]. Emerging research has implicated various microglial signaling pathways in this process, many of which are reactivated later in life in different neurological disorders [15,16,28]. For example, pathological involvement of the CR3 synaptic pruning pathway has been implicated in Alzheimer's disease, frontotemporal dementia, and schizophrenia [15,16,29]. CX3CR1 signaling is implicated in epilepsy and sensory-lesion-induced synaptic pruning [14,30]. Given the induction of both the CR3 and CX3CR1 pathways in the spinal cord after nerve injury, we explored the possibility of their involvement in the remodeling of dorsal horn circuits in neuropathic pain. The evidence for a role of the CR3 synapse pruning pathway in neuropathic pain was abundant, as specific disruptions at multiple levels of this pathway protected both dorsal horn inhibitory and excitatory synapses and prevented synapse engulfment. Unlike the CR3 pathway, the CX3CR1 pathway did not appear to play a significant role in dorsal horn synapse pruning. The modest reduction in engulfment of excitatory synapses in neuropathic CX3CR1 KO mice can be explained by other defects in CX3CR1-deficient microglia [31,32]. These include the interference with basic homeostatic functions such as cell adhesion and motility that affect the phagocytic activity of microglia required for synapse pruning [31,32].

Apart from synapse pruning pathways, phagocytosis-related receptors, such as P2Y12, P2Y6, and TMEM16F, were reported to be upregulated in neuropathic pain and pharmacological blockade or

genetic deletion of these receptors were shown to reduce neuropathic pain [33-35]. Many of these receptors have been implicated in synapse removal in other contexts [36,37]. While we cannot rule out the possibility that these pathways might also contribute to dorsal horn synapse removal in neuropathic pain, our data indicate that the CR3 pathway has a central role in this process. The complete protection of the dorsal horn synaptic network in C3 KOs and in mice treated with a C1q inhibitor supports the notion that the CR3 pathway is necessary for spinal synaptic remodelling in neuropathic pain.

Microglia rewire dorsal horn circuitry in neuropathic pain

Our data demonstrate that microglia reorganize dorsal horn synaptic circuitry in neuropathic conditions through the CR3-dependent signaling pathway. This function of microglia results in two key changes in the dorsal horn synaptic network: 1) a major deficit in inhibitory synapses; 2) reorganization of excitatory synapses without an apparent decrease in excitatory synapse density. In contrast to what was observed in inhibitory synapses, the elevated engulfment of excitatory synaptic terminals, although smaller than the engulfment of inhibitory synapses, did not lead to a net loss of excitatory synapses. This suggests that a compensatory mechanism, specific to the excitatory system, is in place to replenish excitatory synapses. Interestingly, blocking engulfment results in an increase in excitatory synapse density that unmasks the dynamic process of excitatory synapse formation in the spinal cord. This is consistent with emerging studies demonstrating activity-dependent excitatory synaptogenesis as a contributing mechanism to neuropathic pain [38,39]. Interestingly, the dynamics of dorsal horn excitatory synapses in neuropathic pain resembles the later phase of development when excitatory synaptogenesis accompanies synapse pruning [40]. Much like development, in neuropathic pain, spinal inhibition is highly compromised, and the spinal cord microenvironment is fueled with neurotrophic and neuromodulating factors to support excitatory plasticity [6,41,42].

One of the fundamental pathological features of neuropathic pain is the imbalance between excitation and inhibition of dorsal horn neuronal circuits [43,44]. In this study, we provided a neuroanatomical basis for this imbalance, which is mediated by synaptic pruning activity of reactive microglia. At the molecular level, our results show that C1q deposition on synapses is necessary for the recruitment of microglia to the synapse. Interestingly, we found that within the spinal cord of neuropathic mice, C1q has a greater preference for inhibitory synapses compared to excitatory synapses. It is possible that differential changes in neuronal activity between inhibitory and excitatory dorsal horn neurons trigger cell type-specific expression of C1q receptors or other recognition molecules at the synapse site [25,27,45]. This preferential removal of inhibitory synapses, in addition to the failure of the inhibitory system to compensate for the net synapse loss, could contribute to the imbalance between inhibition and excitation, leading to increased excitability in neuropathic pain. This is particularly important for the generation of central sensitization, an enhancement in the activity of nociceptive pathways in response to sensory stimuli [46]. Future studies are necessary to uncover the connection between neuronal activity and production of signaling molecules that attract C1q to the synapse site in neuropathic pain.

Targeting C1q interferes with the maintenance of neuropathic pain

Importantly, we showed that chronic inhibition of C1q is effective at reducing neuropathic pain only at the 21 days post-SNI. The delayed effect of anti-C1q antibody treatment suggests that the structural remodeling of the dorsal horn synaptic circuitry is important for the maintenance but not initiation of neuropathic pain. Moreover, despite the robust effects of inhibiting C1q in reducing mechanical hypersensitivity in neuropathic mice, it is important to note that inhibition of C1q does not fully eliminate neuropathic pain behavior. The aberrant increase of excitatory synapses in the anti-C1q-treated group may contribute to the incomplete reversal of pain behavior. To explore this possibility, both

synaptogenesis and synapse pruning pathways should be inhibited at the same time. This would require new genetic tools to allow the selective and simultaneous manipulation of both pathways.

There is growing evidence to support the existence of sexual dimorphism in key microglial pathways implicated in neuropathic pain [47-49]. However, we did not find any obvious sex differences in the CR3-mediated pathway as inhibiting C1q was effective at reducing pain in both male and female mice. This suggests that the sexually dimorphic role of spinal microglia in pain is likely due to the contribution of distinct microglial signaling pathways to sensory symptoms at a given time.

In summary, our results highlight the importance of microglia and the CR3-mediated synapse pruning pathway in the pathological inhibitory synapse loss in neuropathic pain. Targeting components of this pathway, such as the complement proteins, protects dorsal horn circuitry and prevents the maintenance of neuropathic pain.

METHODS

Animals

All mouse experiments were approved by the Animal Care Committee at McGill University and complied with the Canadian Council on Animal Care guidelines. Following weaning, all mice were housed with their same-sex littermates and were kept in a temperature- and humidity-controlled room with a 12-h light/dark cycle and received food and water *ad libitum*. Wildtype C57BL/6 mice (6-8 weeks of age) of both sexes were purchased from The Jackson Laboratory (Bar Harbor, ME) for pharmacology experiments and used to breed mice of both sexes in-house for all remaining experiments. Mice expressing TdTomato under the inhibitory neuron-specific Gad2 promoter (Gad2-tdTom) were generated by crossing Rosa26LSL-tdTomato reporter mouse line (Ai14) (JAX, stock #007908) with Gad2-IRES-Cre mice (JAX, stock #019022). Mice expressing TdTomato under the Tac1 promoter (Tac1-tdTom) were generated by crossing Rosa26LSL-tdTomato reporter mouse line (Ai14) (JAX, stock #007908) with

Tac1-IRES2-Cre-D mice (JAX, stock #021877). Knock-out (KO) mouse lines include homozygous C3 KO (JAX, stock #003641), and Cx3cr1^{GFP} KO (JAX, stock #005582), which were bred in-house.

Pain behavior

Baseline hind paw withdrawal thresholds and the temporal development of mechanical hypersensitivity in mice were assessed using von Frey filaments and the up-down method of Dixon [50]. Mice were placed inside Plexiglas cubicles (5.3x8.5x3.6 cm) with a perforated metal floor and were permitted to habituate for at least 1 hour prior to testing. Mice were tested using an ascending series of von Frey filaments, starting with the lowest filament (0.008 g) until threshold was reached. In this approach, filaments were applied to the plantar surface of the hind paw for 3 seconds and responses were recorded. At least 2 consecutive measures were taken on each hind paw and averaged. The 50% response threshold was then calculated using the formula: 50% threshold (g) = $10^{(X+kd)}/10^4$, where X = the value (in log units) of the final von Frey filament, k = tabular value for the response pattern and d = the average increment (in log units) between von Frey filaments. All experiments took place during the light cycle and male and female animals were tested on separate days. All experimenters were blinded to the genotype of the mouse and/or the treatment group.

Peripheral nerve injury surgery

In all experiments, mice received a spared nerve injury (SNI) on the left/ipsilateral side, which was performed under isoflurane/oxygen anesthesia as previously described [51]. For this, the sciatic nerve was exposed after making an incision on the skin on the lateral surface of the mouse thigh and sectioning through the biceps femoris muscle. Two of the three terminal branches of the sciatic nerve were tightly ligated with 7.0 silk (Covidien, S-1768K) and 2–4 mm of the nerve distal to the ligation were removed, avoiding any disturbance of the spared nerve. The muscle and skin were closed in separate layers using

coated Vicryl (Ethicon, J489G). For experiments in which the sural nerve was left intact, von Frey testing was performed on the lateral part of the hind paw. In one experiment in which the tibial nerve was intact, von Frey filaments were targeted to the mid-plantar hind paw [52]. In all experiments mice were retested for mechanical hypersensitivity every 7 days for 3 weeks.

Drugs

PLX3397 (Selleckchem) (30 mg/kg, intraperitoneally (i.p), daily) was dissolved in 10% DMSO + 45% PEG 300 + 5% tween 80 + ddH_2O at 20 mg/ml and administrated for 6 consecutive days. For the C1q neutralizing antibodies experiment, animals received i.p injections of either the ANX-M1.21 anti-C1q function blocking antibody (kindly provided by Annexon Biosciences) or IgG isotype control (provided by Annexon Biosciences) at 100 mg/kg every 4 days starting 1 day prior to peripheral nerve injury until the experimental endpoint.

Tissue preparation and immunohistochemistry

At different time points post-surgery, for immunohistochemistry analyses, mice were anaesthetised (0.3 ml/100 g of body weight of Equithesin containing 6.5 mg of chloral hydrate and 3 mg sodium pentobarbital), and perfused transcardially with perfusion buffer (0.5 g/L $NaHCO_3$ in PBS) followed by 4% paraformaldehyde (PFA) in 0.1 M phosphate buffer (PB), pH 7.4, for 10 min. After fixation, spinal cords were extracted and post-fixed in the same fixative overnight at 4 °C and then transferred to 30% sucrose in PB for cryoprotection. For immunohistochemistry, transverse spinal cord sections from the lumbar enlargement (L3–L5) were cut on a cryostat (Leica, Germany) at −20 °C. Twenty-µm-thick sections were prepared for Airyscan confocal microscopy (Carl Zeiss LSM 880) and 10-µm-thick sections were prepared for structural illumination microscopy (SIM) (DeltaVision OMX SR). Sections were then permeabilized and blocked at room temperature for 1 hour in 10% normal donkey or goat

serum and 0.2% Triton-X in PBS (PBST). This step was followed by incubation of sections in a cocktail of primary antibodies in 5% blocking solution at 4 °C. Primary antibodies were rabbit anti-Iba1 (Wako 019-19741, 1:1000), guinea pig anti-Iba1 (Synaptic Systems 234 004, 1:500), rat anti-CD68 (Bio-Rad NBP2-33337, 1:500), mouse anti-vesicular GABA transporter (VGAT, Synaptic Systems 131 011BT, 1:1000), rabbit anti-VGAT (Synaptic Systems 131 008, 1:2000), rat anti-CD11b (Bio-Rad MCA711, 1:100), guinea pig anti-VGLUT2 (Millipore AB2251-I, 1:2000), mouse anti-gephyrin (Synaptic Systems 147 011, 1:400), rabbit anti-Homer1 (Synaptic Systems 160 003, 1:200), goat anti-mouse C3 (MP Biomedicals 55444, 1:100), rabbit-anti NeuN (Millipore 32160702, 1:1000), rabbit anti-C1q (Abcam 182451, 1:400), goat anti-CX3CL1 (R&D systems AF 537, 1:500), and rabbit anti-CX3CR1 (Thermofisher TP501, 1:200). Twenty-four hours later, appropriate Alexa-fluorophore-conjugated secondary antibodies were applied to sections (Invitrogen, 1:800), which were incubated at room temperature for 2 hours. In some experiments, isolectin B4 (IB4) conjugated to Alexa 647 fluorophore was used in the mixture of secondary antibodies (Invitrogen, 1:200). Sections were then mounted and coverslipped using Prolong Gold Antifade mounting medium (Invitrogen) and Zeiss cover slips.

Microglia density quantification

Low magnification images were captured using a Zeiss AxioImager M2 Imaging microscope with the Zeiss ZenPro software v.2.3 (Zeiss Canada). For quantification of microglia density, 4 sections per animal were assessed. To capture the entire dorsal horn, a 10X field was imaged. To calculate the density of microglia, the number of microglia was divided by the area of the dorsal horn measured using ImageJ software (NIH).

Engulfment quantification

For assessing phagocytosis of synaptic elements, we used an engulfment quantification method inspired by Schafer and colleagues [53]. Briefly, sections immunolabeled with CD68, Iba1, and a marker for the neuronal structure of interest were imaged by 63x oil immersion objective (NA 1.4) at 0.2 µm z-steps using a Zeiss LSM 800 Airyscan confocal microscope. Images were processed with IMARIS software (Bitplane) to produce 3D surface renderings of the engulfed material within microglial lysosomes, microglia, and lysosomes. Volumes associated with each surface rendered structure were recorded and engulfment measurements for each microglial cell were calculated using the formula: the volume of the engulfed material within lysosomal compartments/the volume of microglial cell. For each animal, graphed values represent the mean of a total of 8 - 12 microglia sampled from 4 sections analyzed. Only microglia that had their full cell bodies imaged were selected for quantification. Imaging parameters, selection criteria, and thresholding values were consistently applied to all quantifications. All experimenters were blinded to the genotype of the mouse, sex, and/or the treatment condition. Blinding to laterality in untreated mice was not possible because of the evident morphological changes in ipsilateral microglia.

Analysis of synaptic elements

SIM was used to assess synapse densities. Cells were imaged with a 100x, NA = 1.42, oil immersion objective on a Vision OMX V_4 Blaze system (GE) equipped with 488 nm, 592 nm, and 647 nm lasers and two Evolve EM-CCD cameras (Photometrics, Huntington Beach, CA, USA). Image stacks of 2 µm were reconstructed in Deltavision softWoRx 6.1.1 software with a Wiener filter of 0.01 using channel-specific optical transfer functions [54]. Captured synapses were analyzed using Colocalize Spots MATLAB function on IMARIS. A synapse was counted if the distance between the center point of a presynaptic and postsynaptic puncta was equal to or less than the radius of the presynapatic puncta + 0.1 µm, an empirically determined scaling factor [55]. All experiments were analyzed blind to groups.

RNA-seq analysis

Transcriptomics data of spinal cord from naive mice and SNI-injured mice was taken from Gene Expression Omnibus accession GSE111216 [22]. In short, RNA-Seq data have been trimmed with Trimmomatic v0.32 [56], then mapped on UCSC's mouse genome version mm10 grabbed from ftp://ussd-ftp.illumina.com/Mus_musculus/UCSC/mm10/ using tophat v2.0.11 [57] and bowtie v1.0.0 [58]. Differential gene expression detected at gene level from experimental triplicates using cuffdiff v2.2.1 [59].

RNAscope

The RNAscope Fluorescent Multiplex Assay (ACD Biosystems) was performed according to the ACD protocol for fresh-frozen tissue. Perfusion fixed spinal cords from animals at 7 days after injury were sectioned at 10 µm on a cryostat and hybridized with C1qa mRNA probe (ACD cat#: 441221). The ACD 3-plex served as a negative control and applied on one section per slide to confirm signal specificity. The probes were amplified according to the manufacturer's instructions and labeled with Alexa 488 nm fluorophores.

Experimental design and statistical analyses

Sample sizes were determined based on pilot studies and in the absence of sex differences, male and female animals were pooled. All statistical tests were completed using Windows GraphPad Prism version 8. Analyses used include only parametric tests: one-way ANOVA, two-way repeated measures ANOVA, and two-way ANOVA, followed by Bonferroni's multiple comparison tests. For comparing two groups unpaired or paired two-tailed t-tests were used. All p values and statistical tests employed are indicated in results and figure legends.

ACKNOWLEDGMENTS

This work was funded by Canadian Institutes of Health Research (CIHR) operating grant MOP 136903, and project grant PJT-166195 and Louise and Alan Edwards Foundation (LAEF) to ARS. YDK was supported by a Canada Research Chair in Chronic Pain and related Brain Disorders. We are thankful to Dr. Masha Prager-Khoutorsky and McGill University Life Science Complex ABIF for their technical support. We also thank Dr. Ji Zhang for kindly giving us the CX3CR1 KO mouse line.

AUTHOR CONTRIBUTIONS

NY designed and planned the entire study with the help of ST and SL. NY carried out the majority of the experiments, prepared the figures and wrote the manuscript. ST designed and performed ANX M1.21 behavior experiments. BS and JSA performed neuropathic pain surgeries. JSA performed genetic data analysis. VB, VCC, MSL, HD and KL assisted with the histology experiments. HD proofread the manuscript. CW (Wang) performed a portion of engulfment and synapse quantifications. CW (Wong) assisted with transgenic mice colonies and proofread the manuscript. AK supported the super-resolution microscopy, transgenic studies, and contributed to manuscript editing. VM, TY and YAZ contributed to the design of the ANX M1.21 component of the study. YDK and LD contributed to the overall idea and manuscript reviewing. PS and JM edited the manuscript. ARS oversaw the project as a whole and edited the manuscript.

DECLARATION OF INTERESTS

The authors have declared that no conflict of interest exists.

FIGURES

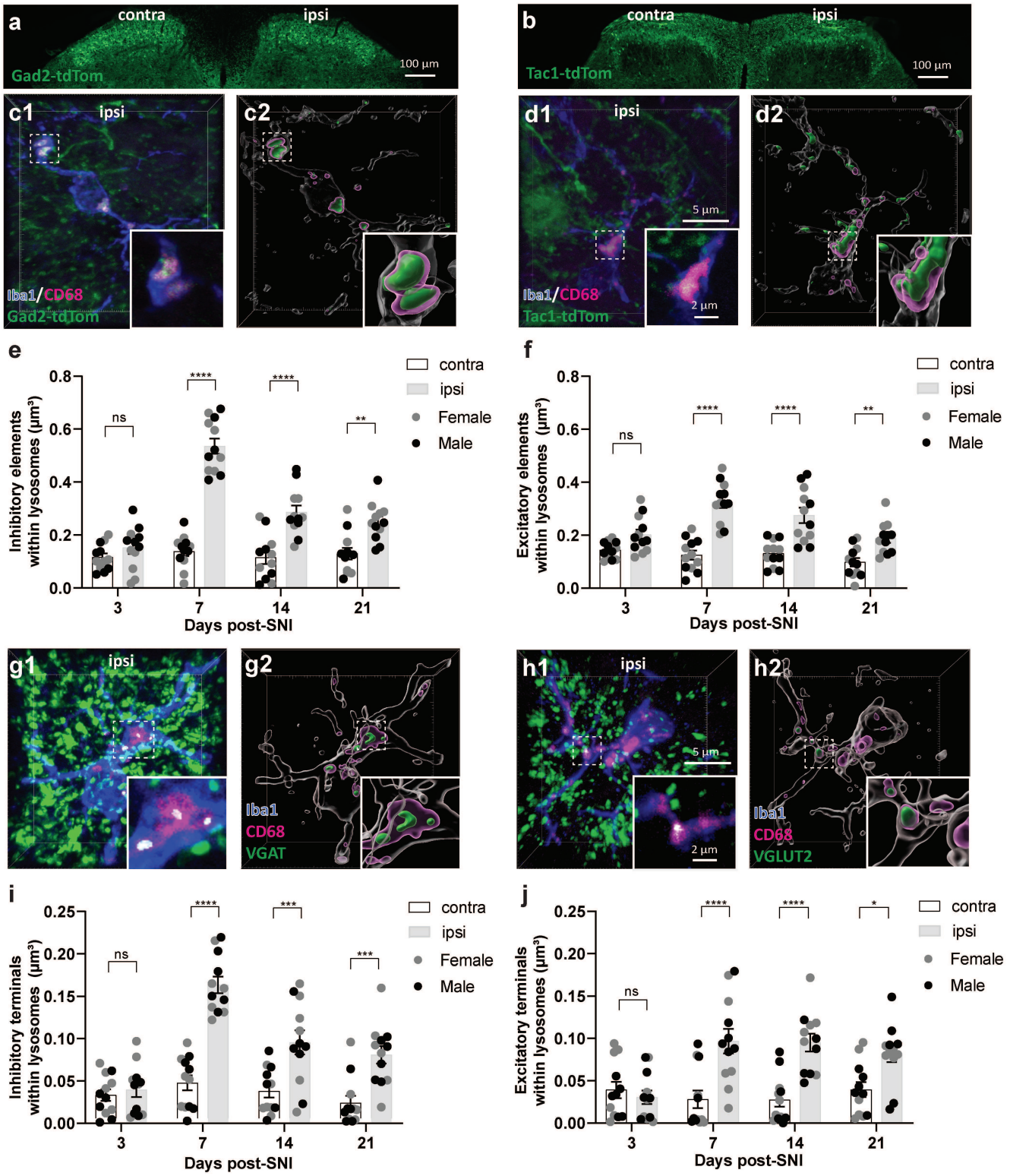

Figure 1. Nerve injury triggers engulfment of presynaptic terminals by microglia

a-**b** The expression of tdTomato fluorescent protein reporter in dorsal horn of Gad2-tdTom (**a**) and Tac1-tdTom (**b**) mice to demonstrate the distributions of inhibitory Gad65-expressing and excitatory substance

P-expressing neurons, respectively. **c-d** Representative 3D reconstructions (**c1**, **d1**) and surface rendering (**c2**, **d2**) of microglia (blue) sampled from ipsilateral dorsal horn (lamina II) to show internalized inhibitory and excitatory neuronal elements within lysosomal compartments (magenta) of ipsilateral microglia. Insets within raw images are single plane enlarged images selected from confocal stacks illustrating the presence of tdTomato fluorescent signals inside lysosomes. Insets within 3D reconstructions are enlarged views of the engulfed volumes from the same regions. **e-f** Quantification of temporal changes of engulfment of inhibitory (**e**) and excitatory (**f**) $tdTomato^{+}$ neuronal structures by microglia (n = 12 per group; 6 per sex). **g-h** Three-dimensional fluorescent images of microglia (blue) from ipsilateral dorsal horn labeled for lysosomal marker CD68 (magenta), marker of presynaptic inhibitory terminals (VGAT; green) (**g1**) and marker of presynaptic excitatory terminals (VGLUT2; green) (**h1**). Representative 3D surface-rendered images illustrate the engulfment of presynaptic elements (**g2** and **h2**). **i-j** Quantification of temporal changes of engulfment of inhibitory (**i**) and excitatory (**j**) presynaptic terminals by microglia (n = 12 per group; 6 per sex). *$p < 0.05$, **$p < 0.01$, ***$P < 0.001$, and ****$P < 0.0001$ analyzed with two-way ANOVA followed by Bonferroni post hoc test. Means are plotted with individual data points ± SEM.

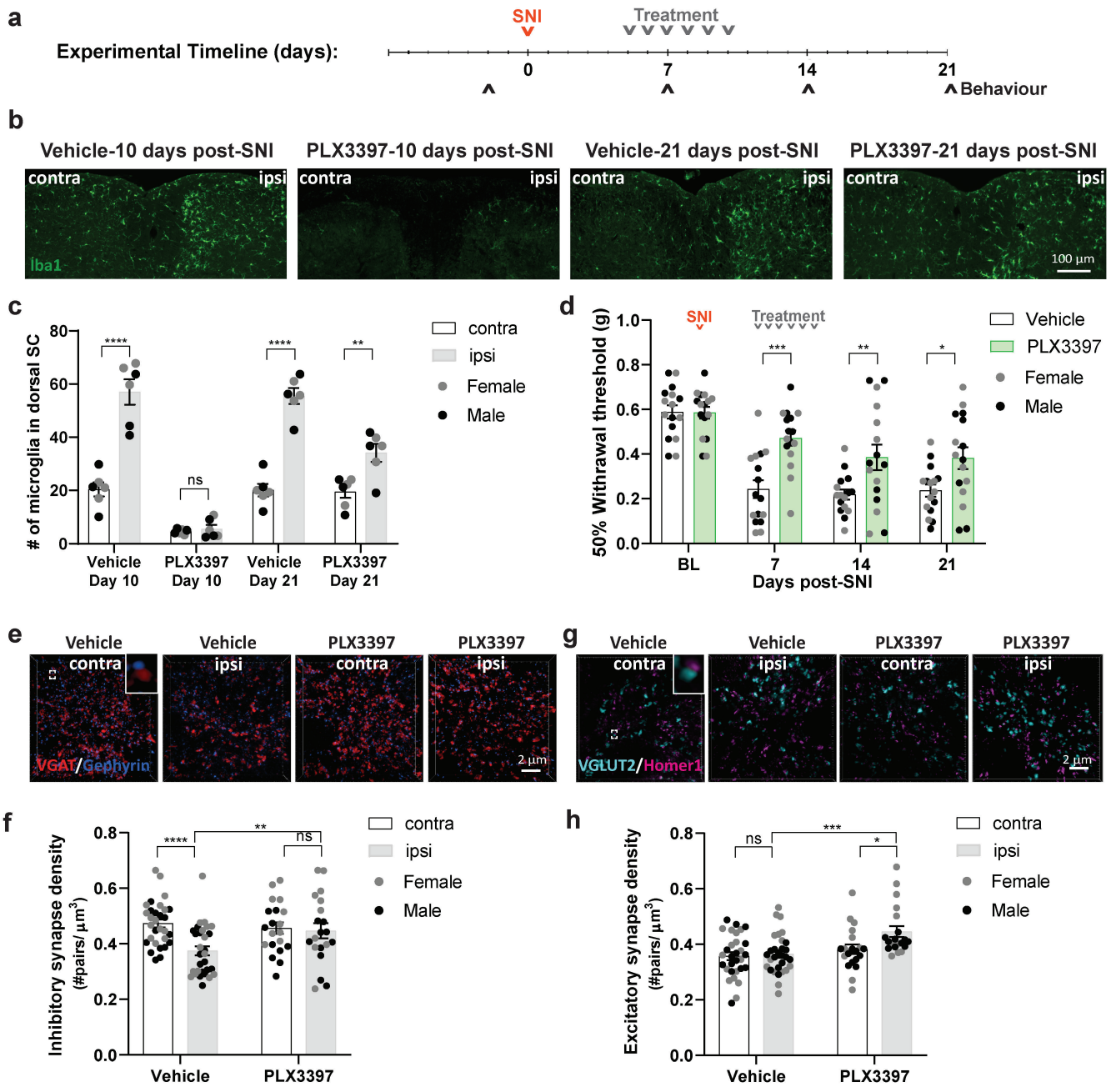

Figure 2. Transient microglia depletion during the peak of synapse engulfment prevents the normal development of mechanical hypersensitivity and protects dorsal horn synaptic connectivity. a An experimental diagram showing the timeline of drug treatments, SNI surgery, and behavioral tests. **b** Dorsal horn images labeled for Iba1 (green) from vehicle and drug (PLX3397) treated groups from the last day of treatment and after a 10-day wash-out period. **c** Quantification of the number of microglia in dorsal spinal cord (n = 6 per group; 3 per sex). **d** Pain behavior in neuropathic mice treated either with PLX3397 or vehicle (n = 16 per group; 8 per sex). **e** Representative SIM images of inhibitory synapses labeled with a pre-synaptic marker (VGAT; red) and a post-synaptic marker (gephyrin; blue) in different conditions. The inset within the first image is an enlarged view of an inhibitory synapse. **f** Quantification of inhibitory synapse density (n = 20-30 per group; 10-15 per sex). **g** Representative SIM images of excitatory synapses labeled with a pre-synaptic marker (VGLUT2; cyan) and a post-synaptic (homer1; magenta) in different conditions. The inset within the first image is an enlarged view of an

excitatory synapse. **h** Quantification of inhibitory synapse density (n = 20-30 per group; 10-15 per sex). *p < 0.05, **p < 0.01, ***p < 0.001 and ****p < 0.0001 analyzed with repeated measures two-way ANOVA with Bonferroni post hoc test (D) and two-way ANOVA with Bonferroni post hoc test (**c**, **f**, and **h**). Means are plotted with individual data points ± SEM.

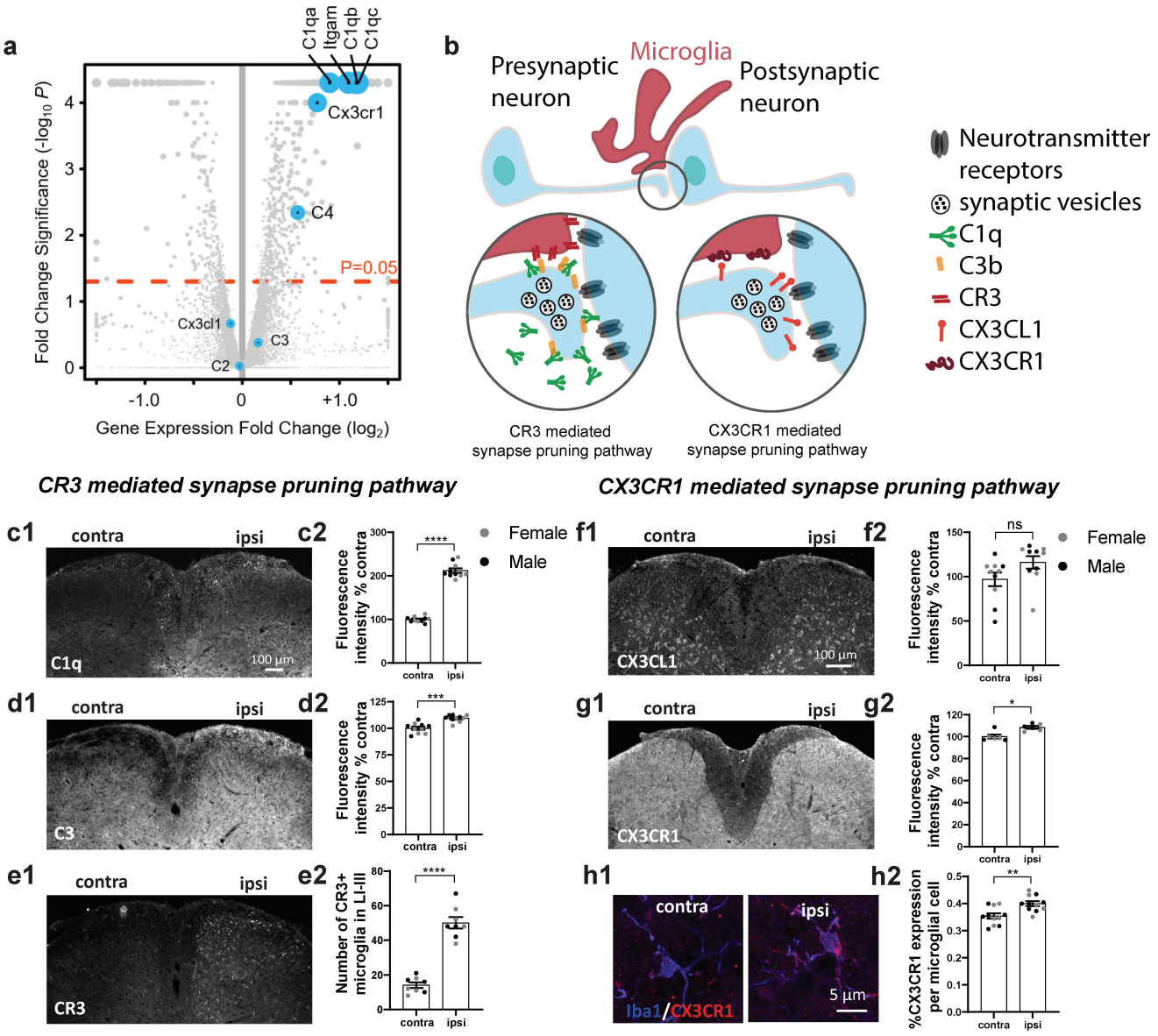

Figure 3. CR3 and CX3CR1 mediated synapse pruning pathways are upregulated in neuropathic pain. a Volcano plot showing gene expression changes in neuropathic mice at day 7 post SNI. Each dot is a gene. Positive fold change indicates higher expression in the spinal cord of SNI-injured mice than in naïve. Genes highlighted in blue are related to CR3 and CX3CR1 pruning pathways. Dashed horizontal orange line indicates P-value of 0.05. **b** The schematic illustrates microglia and signaling molecules that participate in CR3 and CX3CR1 pruning mechanisms. **c1-e1** Representative images of C1q, C3, and CR3 labeling in the dorsal horn of SNI mice 7 days after injury. **c2-e2** Quantifications of fluorescence intensity of dorsal horn C1q, and C3, as well as number of $CR3^{+}$ microglia in laminae I-III (n = 8 per group; 4 per sex). **f1** Representative dorsal horn image of CX3CL1 immunolabelling in SNI mice 7 days after injury (quantified in **f2**) (n = 8 per group; 4 per sex). **g1** Low-magnification representative images of CX3CR1 expression in the dorsal horn of SNI mice (quantified in **g2**) (n = 8 per group; 4 per sex). **h1** High-resolution image of CX3CR1 (red) expression in microglia (blue) sampled from ipsilateral and contralateral dorsal horn (quantified **h2**) (n = 8 per group; 4 per sex). **p < 0.01, ***p < 0.001, and ****p < 0.0001 analyzed with paired two-tailed t-test (**c2-g2**) and unpaired t-test (**h2**). Means are plotted with individual data points ± SEM.

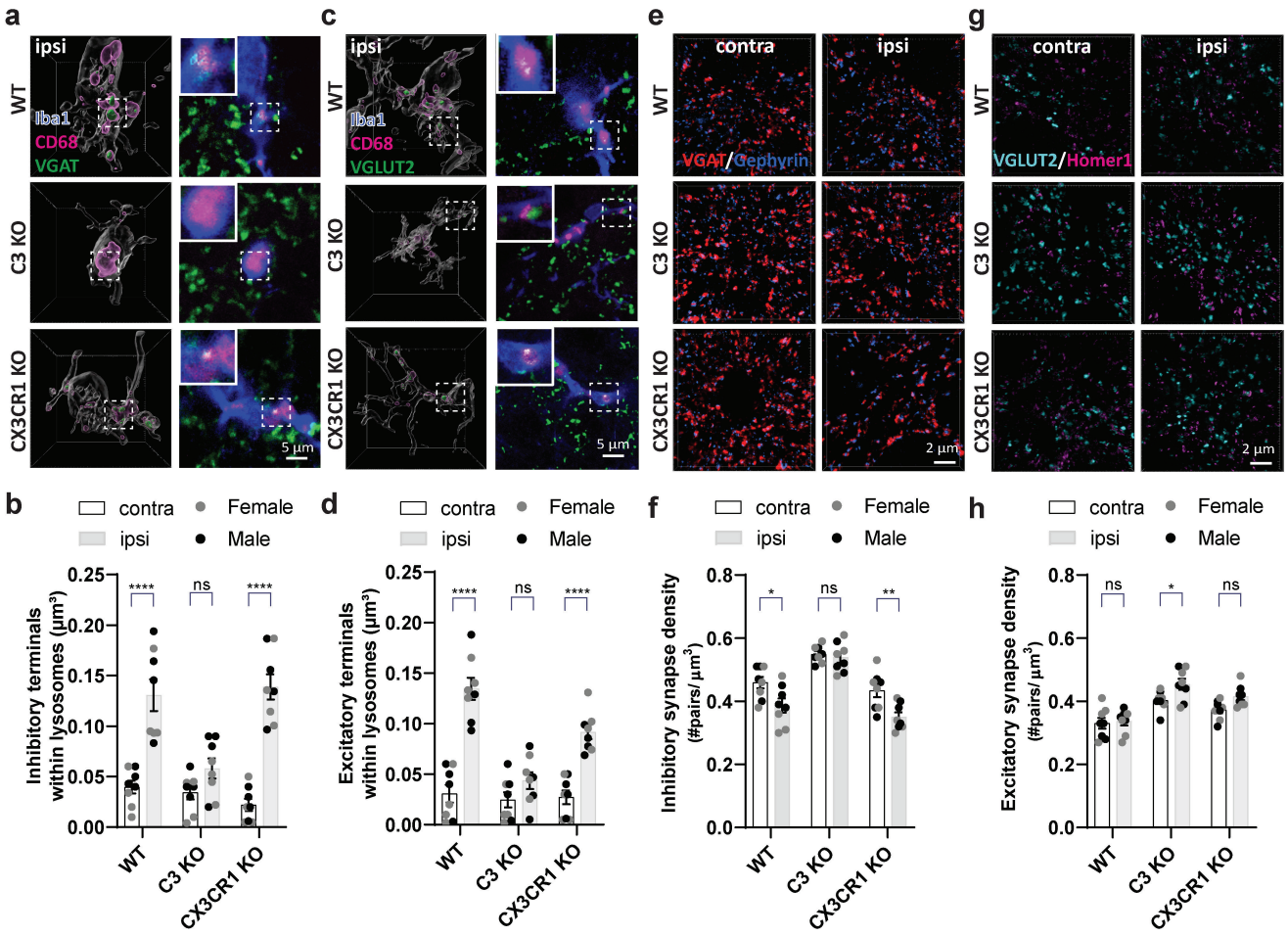

Figure 4. Nerve injury induced engulfment of spinal presynaptic terminals is mediated by CR3 pathway. a and **c** Images in the first column are representative surface rendering 3D reconstructions of microglia (white) sampled from ipsilateral dorsal horns of neuropathic wildtype (WT), C3 KOs, and CX3CR1 KOs and demonstrate lysosome (magenta) co-localization with $VGAT^+$ inhibitory (**a**) and $VGLUT2^+$ excitatory (**c**) pre-synaptic markers (green). Single plane images selected from confocal stacks illustrating the presence or absence of $CD68^+$ lysosomal co-localization with synapse markers are shown in the second column. **b** and **d** Quantifications of engulfment of inhibitory (**b**) and excitatory (**d**) presynaptic terminals by microglia in different genotypes (n = 8 per group; 4 per sex). **e** and **g** Three-dimensional SIM representative images of inhibitory (**a1**: VGAT in red and gephyrin in blue) and excitatory (**b1**: VGLUT2 in cyan and homer1 in magenta) terminals captured from ipsilateral and contralateral dorsal horns of WT, C3 KO, and CX3CR1 KO neuropathic mice. **f** and **h** Quantifications of dorsal horn inhibitory (**f**) and excitatory (**h**) synapse densities for neuropathic mice of different genotypes (n = 8 per group; 4 per sex). *$p < 0.05$, **$p < 0.01$, and ****$p < 0.0001$ analyzed by two-way ANOVA with Bonferroni post hoc test. Means are plotted with individual data points ± SEM.

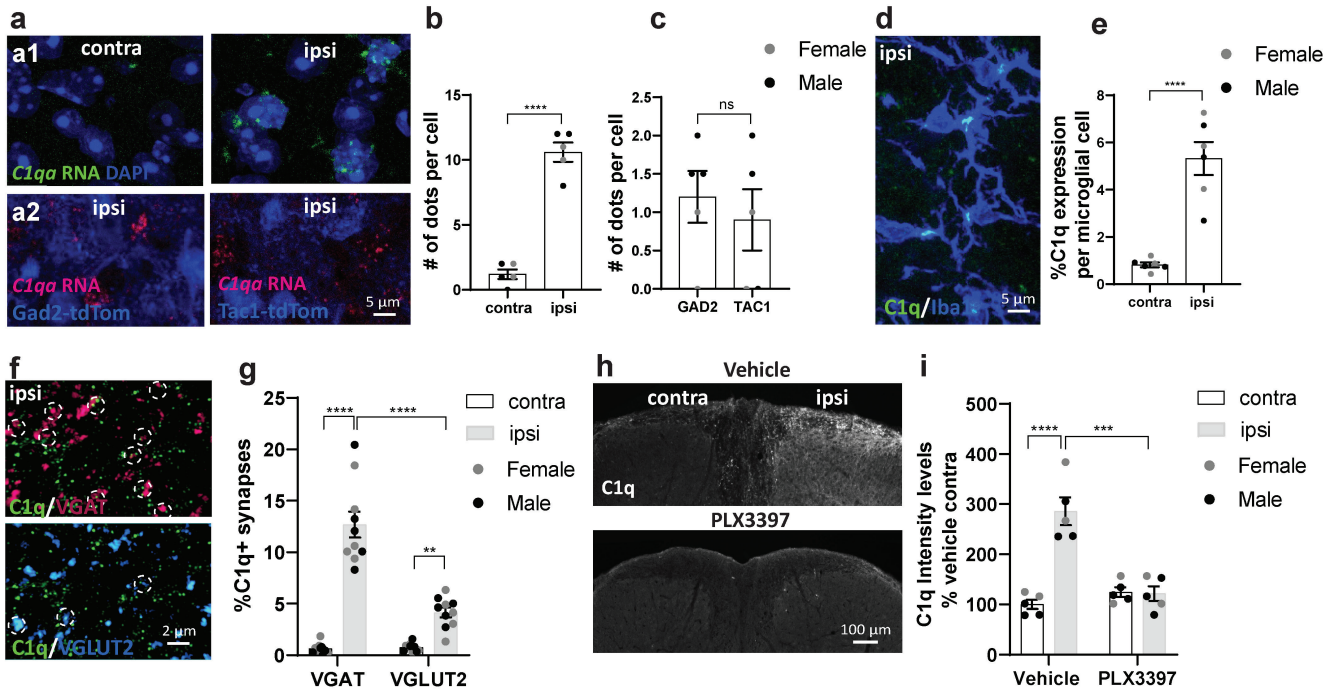

Figure 5. Complement protein C1q is expressed by nerve injury-activated microglia and localized to dorsal horn synapses. a RNA scope for *C1qa* (**a1**: green) in ipsilateral and contralateral dorsal horn cells (quantified in **b**) (n = 5 per group; 2-3 per sex). Absence of *C1qa* (**a2**: red) expression in inhibitory and excitatory substance P^+ neurons (blue) (quantified in **c**) (n = 5 per group; 2-3 per sex). **d** Representative high-magnification confocal image of C1q protein (green) in microglia (blue) (quantified in **e**) (n = 6 per group; 3 per sex). Dotted circle shows an example of extracellular C1q protein (enlarged view shown in the inset). Representative SIM images (**f**) captured from ipsilateral dorsal horn at 7 days after injury show the preferential co-localization of C1q (green) with inhibitory synapses (VGAT in red), compared to excitatory (VGLUT2 in blue). Dotted circles show synapses that are colocalized with C1q. **g** Quantifications of C1q co-localization with inhibitory and excitatory synapses (n = 10 per group; 5 per sex). **h** C1q staining patterns in the dorsal horn of neuropathic mice chronically treated with vehicle and PLX3397 (quantified in **i**) (n = 6 per group; 3 per sex). **j** Quantifications of C1q co-localization with inhibitory and excitatory synapses in vehicle and PLX3397 treated mice. ***p < 0.001, and ****p < 0.0001 analyzed by two-way ANOVA with Bonferroni post hoc test (**g**, **i-j**) and unpaired t-test (**b-c**, and **e**). Means are plotted with individual data points ± SEM.

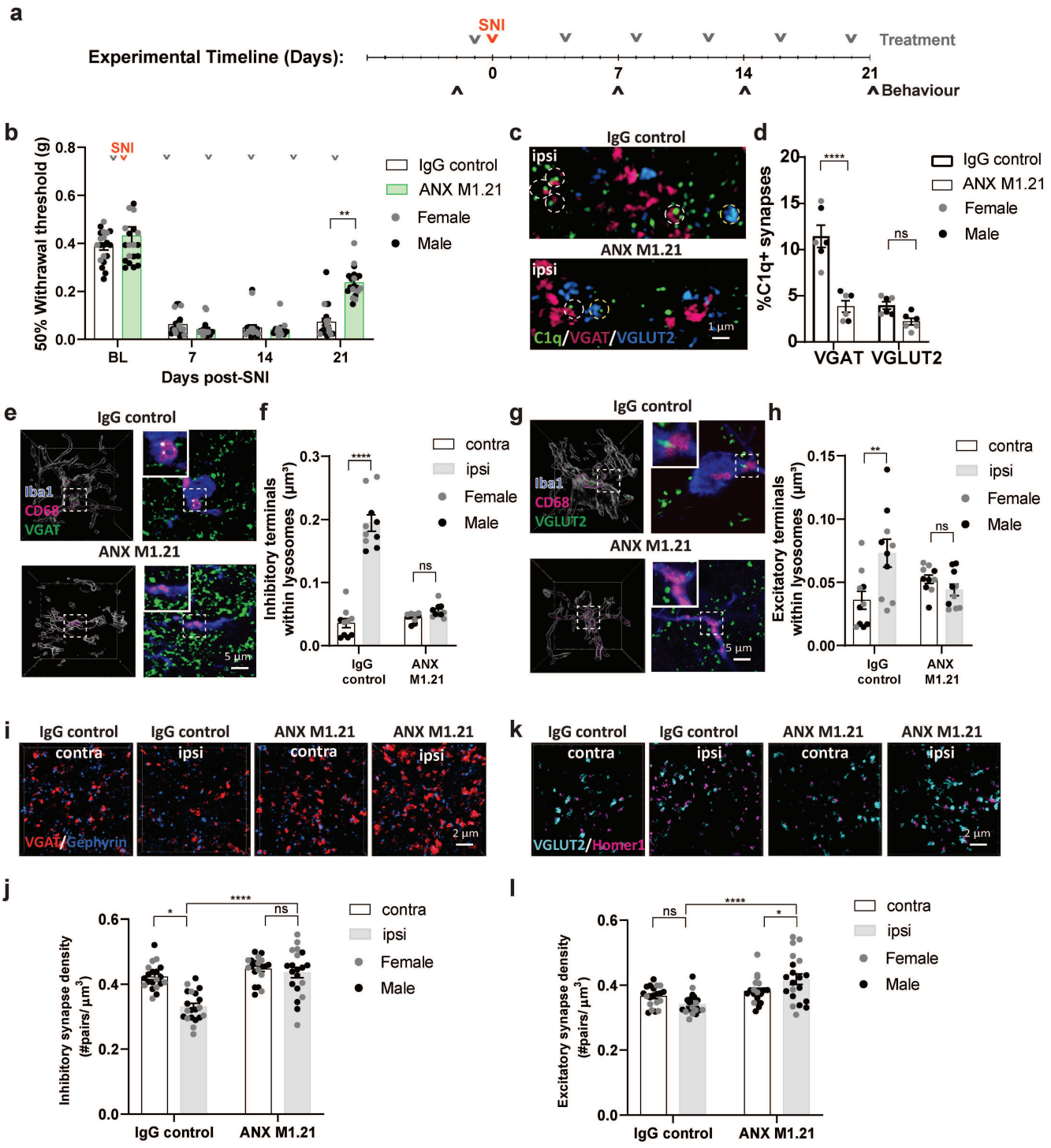

Figure 6. Functional blocking of C1q alleviates mechanical hypersensitivity, reduces synapse pruning, and prevents dorsal horn synapse loss. a A diagram showing the timeline of drug treatments, surgery, and behavior test. **b** Pain behaviour in neuropathic mice treated either with ANX-M1.21 or IgG control (n = 20 per group; 12 male and 8 female). **c** Representative images from ipsilateral dorsal horn show the co-localization of C1q (green) with inhibitory synapses (VGAT; red), and excitatory (VGLUT2; blue) in different experimental groups (Quantified in **d**) (n = 6 per group; 3 per sex). **e** and **g** Representative 3D surface rendering of microglia (white) from ipsilateral dorsal horn of IgG control and ANX-M1.21 treated mice. A single plane enlarged image selected from the confocal stack illustrating

the CD68 (magenta) co-localization with VGAT or VGLUT2 (**e**, **g**: green). Insets within 3D reconstructions are enlarged views of VGAT (**e**) or VGLUT2 (**g**) co-localization with CD68 (quantified in **f** and **h**) (n = 10 per group; 5 per sex). **i** Representative images of inhibitory presynaptic (VGAT; red) and postsynaptic (gephyrin; blue) elements from different conditions and quantification in **j** (n = 20 per group; 12 male and 8 female). **k** Representative images of excitatory pre-synaptic (VGLUT2; cyan) and post-synaptic (homer1; magenta) elements from different conditions and quantification in **l** (n = 20 per group; 12 male and 8 female). *$p < 0.05$, **$p < 0.01$, and ****$p < 0.0001$ analyzed with repeated measures two-way ANOVA with Bonferroni post hoc test (**b**) and two-way ANOVA with Bonferroni post hoc test (**d**, **f**, **h**, **j**, and **l**). Means are plotted with individual data points ± SEM.

REFERENCES

1 Costigan, M., Scholz, J. & Woolf, C. J. Neuropathic pain: a maladaptive response of the nervous system to damage. *Annu Rev Neurosci* **32**, 1-32, doi:10.1146/annurev.neuro.051508.135531 (2009).

2 Baron, R., Binder, A. & Wasner, G. Neuropathic pain: diagnosis, pathophysiological mechanisms, and treatment. *Lancet Neurol* **9**, 807-819, doi:10.1016/S1474-4422(10)70143-5 (2010).

3 Inoue, K. & Tsuda, M. Microglia in neuropathic pain: cellular and molecular mechanisms and therapeutic potential. *Nat Rev Neurosci* **19**, 138-152, doi:10.1038/nrn.2018.2 (2018).

4 Chen, G., Zhang, Y.-Q., Qadri, Y. J., Serhan, C. N. & Ji, R.-R. Microglia in pain: detrimental and protective roles in pathogenesis and resolution of pain. *Neuron* **100**, 1292-1311 (2018).

5 Gilmore, S. A. & Skinner, R. D. Intraspinal non-neuronal cellular responses to peripheral nerve injury. *Anat Rec* **194**, 369-387, doi:10.1002/ar.1091940305 (1979).

6 Coull, J. A. *et al.* BDNF from microglia causes the shift in neuronal anion gradient underlying neuropathic pain. *Nature* **438**, 1017-1021, doi:10.1038/nature04223 (2005).

7 Echeverry, S. *et al.* Spinal microglia are required for long-term maintenance of neuropathic pain. *Pain* **158**, 1792-1801, doi:10.1097/j.pain.0000000000000982 (2017).

8 Jeong, H. *et al.* High-resolution transcriptome analysis reveals neuropathic pain gene-expression signatures in spinal microglia after nerve injury. *Pain* **157**, 964-976, doi:10.1097/j.pain.0000000000000470 (2016).

9 Kuner, R. & Flor, H. Structural plasticity and reorganisation in chronic pain. *Nat Rev Neurosci* **18**, 113, doi:10.1038/nrn.2017.5 (2017).

10 Lorenzo, L. E. *et al.* Enhancing neuronal chloride extrusion rescues alpha2/alpha3 GABAA-mediated analgesia in neuropathic pain. *Nat Commun* **11**, 869, doi:10.1038/s41467-019-14154-6 (2020).

11 Neniskyte, U. & Gross, C. T. Errant gardeners: glial-cell-dependent synaptic pruning and neurodevelopmental disorders. *Nat Rev Neurosci* **18**, 658-670, doi:10.1038/nrn.2017.110 (2017).

12 Schafer, D. P. *et al.* Microglia sculpt postnatal neural circuits in an activity and complement-dependent manner. *Neuron* **74**, 691-705, doi:10.1016/j.neuron.2012.03.026 (2012).

13 Paolicelli, R. C. *et al.* Synaptic pruning by microglia is necessary for normal brain development. *Science* **333**, 1456-1458, doi:10.1126/science.1202529 (2011).

14 Gunner, G. *et al.* Sensory lesioning induces microglial synapse elimination via ADAM10 and fractalkine signaling. *Nat Neurosci* **22**, 1075-1088, doi:10.1038/s41593-019-0419-y (2019).

15 Hong, S. *et al.* Complement and microglia mediate early synapse loss in Alzheimer mouse models. *Science* **352**, 712-716, doi:10.1126/science.aad8373 (2016).

16 Lui, H. *et al.* Progranulin Deficiency Promotes Circuit-Specific Synaptic Pruning by Microglia via Complement Activation. *Cell* **165**, 921-935, doi:10.1016/j.cell.2016.04.001 (2016).

17 Clark, A. K. & Malcangio, M. Fractalkine/CX3CR1 signaling during neuropathic pain. *Front Cell Neurosci* **8**, 121, doi:10.3389/fncel.2014.00121 (2014).

18 Griffin, R. S. *et al.* Complement Induction in Spinal Cord Microglia Results in Anaphylatoxin C5a-Mediated Pain Hypersensitivity. *The Journal of Neuroscience* **27**, 8699-8708, doi:10.1523/jneurosci.2018-07.2007 (2007).

19 Dickie, A. C. *et al.* Morphological and functional properties distinguish the substance P and gastrin-releasing peptide subsets of excitatory interneuron in the spinal cord dorsal horn. *Pain* **160**, 442 (2019).

20 Peirs, C. & Seal, R. P. Neural circuits for pain: Recent advances and current views. *Science* **354**, 578-584, doi:10.1126/science.aaf8933 (2016).

21 Tsuda, M. Microglia in the spinal cord and neuropathic pain. *J Diabetes Investig* **7**, 17-26, doi:10.1111/jdi.12379 (2016).

22 Parisien, M. *et al.* Genetic pathway analysis reveals a major role for extracellular matrix organization in inflammatory and neuropathic pain. *Pain* **160**, 932-944, doi:10.1097/j.pain.0000000000001471 (2019).

23 Presumey, J., Bialas, A. R. & Carroll, M. C. Complement System in Neural Synapse Elimination in Development and Disease. *Adv Immunol* **135**, 53-79, doi:10.1016/bs.ai.2017.06.004 (2017).
24 Stephan, A. H. *et al.* A dramatic increase of C1q protein in the CNS during normal aging. *Journal of Neuroscience* **33**, 13460-13474 (2013).
25 Bialas, A. R. & Stevens, B. TGF-beta signaling regulates neuronal C1q expression and developmental synaptic refinement. *Nat Neurosci* **16**, 1773-1782, doi:10.1038/nn.3560 (2013).
26 Stevens, B. *et al.* The classical complement cascade mediates CNS synapse elimination. *Cell* **131**, 1164-1178, doi:10.1016/j.cell.2007.10.036 (2007).
27 Gyorffy, B. A. *et al.* Local apoptotic-like mechanisms underlie complement-mediated synaptic pruning. *Proc Natl Acad Sci U S A* **115**, 6303-6308, doi:10.1073/pnas.1722613115 (2018).
28 Yilmaz, M. *et al.* Overexpression of schizophrenia susceptibility factor human complement C4A promotes excessive synaptic loss and behavioral changes in mice. *Nat Neurosci* **24**, 214-224, doi:10.1038/s41593-020-00763-8 (2021).
29 Sekar, A. *et al.* Schizophrenia risk from complex variation of complement component 4. *Nature* **530**, 177-183, doi:10.1038/nature16549 (2016).
30 Ali, I., Chugh, D. & Ekdahl, C. T. Role of fractalkine-CX3CR1 pathway in seizure-induced microglial activation, neurodegeneration, and neuroblast production in the adult rat brain. *Neurobiol Dis* **74**, 194-203, doi:10.1016/j.nbd.2014.11.009 (2015).
31 Sheridan, G. K. & Murphy, K. J. Neuron-glia crosstalk in health and disease: fractalkine and CX3CR1 take centre stage. *Open Biol* **3**, 130181, doi:10.1098/rsob.130181 (2013).
32 Fong, A. M., Alam, S. M., Imai, T., Haribabu, B. & Patel, D. D. CX3CR1 tyrosine sulfation enhances fractalkine-induced cell adhesion. *J Biol Chem* **277**, 19418-19423, doi:10.1074/jbc.M201396200 (2002).
33 Barragan-Iglesias, P. *et al.* Role of spinal P2Y6 and P2Y11 receptors in neuropathic pain in rats: possible involvement of glial cells. *Mol Pain* **10**, 29, doi:10.1186/1744-8069-10-29 (2014).
34 Maeda, M., Tsuda, M., Tozaki-Saitoh, H., Inoue, K. & Kiyama, H. Nerve injury-activated microglia engulf myelinated axons in a P2Y12 signaling-dependent manner in the dorsal horn. *Glia* **58**, 1838-1846, doi:10.1002/glia.21053 (2010).
35 Batti, L. *et al.* TMEM16F Regulates Spinal Microglial Function in Neuropathic Pain States. *Cell Rep* **15**, 2608-2615, doi:10.1016/j.celrep.2016.05.039 (2016).
36 Sipe, G. O. *et al.* Microglial P2Y12 is necessary for synaptic plasticity in mouse visual cortex. *Nat Commun* **7**, 10905, doi:10.1038/ncomms10905 (2016).
37 Koizumi, S. *et al.* UDP acting at P2Y6 receptors is a mediator of microglial phagocytosis. *Nature* **446**, 1091-1095, doi:10.1038/nature05704 (2007).
38 Simonetti, M. *et al.* Nuclear calcium signaling in spinal neurons drives a genomic program required for persistent inflammatory pain. *Neuron* **77**, 43-57, doi:10.1016/j.neuron.2012.10.037 (2013).
39 Yu, Y. P., Gong, N., Kweon, T. D., Vo, B. & Luo, Z. D. Gabapentin prevents synaptogenesis between sensory and spinal cord neurons induced by thrombospondin-4 acting on pre-synaptic Cav alpha2 delta1 subunits and involving T-type Ca(2+) channels. *Br J Pharmacol* **175**, 2348-2361, doi:10.1111/bph.14149 (2018).
40 Tau, G. Z. & Peterson, B. S. Normal development of brain circuits. *Neuropsychopharmacology* **35**, 147-168, doi:10.1038/npp.2009.115 (2010).
41 Coull, J. A. *et al.* Trans-synaptic shift in anion gradient in spinal lamina I neurons as a mechanism of neuropathic pain. *Nature* **424**, 938-942, doi:10.1038/nature01868 (2003).
42 Kaila, K., Price, T. J., Payne, J. A., Puskarjov, M. & Voipio, J. Cation-chloride cotransporters in neuronal development, plasticity and disease. *Nat Rev Neurosci* **15**, 637-654, doi:10.1038/nrn3819 (2014).
43 Inquimbert, P. *et al.* NMDA Receptor Activation Underlies the Loss of Spinal Dorsal Horn Neurons and the Transition to Persistent Pain after Peripheral Nerve Injury. *Cell Rep* **23**, 2678-2689, doi:10.1016/j.celrep.2018.04.107 (2018).
44 Lee, K. Y., Ratte, S. & Prescott, S. A. Excitatory neurons are more disinhibited than inhibitory neurons by chloride dysregulation in the spinal dorsal horn. *Elife* **8**, doi:10.7554/eLife.49753 (2019).

45 Scott-Hewitt, N. *et al.* Local externalization of phosphatidylserine mediates developmental synaptic pruning by microglia. *EMBO J* **39**, e105380, doi:10.15252/embj.2020105380 (2020).
46 Latremoliere, A. & Woolf, C. J. Central sensitization: a generator of pain hypersensitivity by central neural plasticity. *J Pain* **10**, 895-926, doi:10.1016/j.jpain.2009.06.012 (2009).
47 Sorge, R. E. *et al.* Spinal cord Toll-like receptor 4 mediates inflammatory and neuropathic hypersensitivity in male but not female mice. *Journal of Neuroscience* **31**, 15450-15454 (2011).
48 Sorge, R. E. *et al.* Different immune cells mediate mechanical pain hypersensitivity in male and female mice. *Nat Neurosci* **18**, 1081-1083, doi:10.1038/nn.4053 (2015).
49 Taves, S. *et al.* Spinal inhibition of p38 MAP kinase reduces inflammatory and neuropathic pain in male but not female mice: Sex-dependent microglial signaling in the spinal cord. *Brain Behav Immun* **55**, 70-81, doi:10.1016/j.bbi.2015.10.006 (2016).
50 Chaplan, S. R., Bach, F. W., Pogrel, J. W., Chung, J. M. & Yaksh, T. L. Quantitative assessment of tactile allodynia evoked by unilateral ligation of the fifth and sixth lumbar nerves in the rat. *J Neurosci Meth.* **53**, 55–63, doi:10.1016/0165-0270(94)90144-9 (1994).
51 Decosterd, I. & Woolf, C. J. Spared nerve injury: an animal model of persistent peripheral neuropathic pain. *Pain* **87**, 149-158 (2000).
52 Shields, S. D., Eckert, W. A., 3rd & Basbaum, A. I. Spared nerve injury model of neuropathic pain in the mouse: a behavioral and anatomic analysis. *J Pain* **4**, 465-470, doi:10.1067/s1526-5900(03)00781-8 (2003).
53 Schafer, D. P., Lehrman, E. K., Heller, C. T. & Stevens, B. An engulfment assay: a protocol to assess interactions between CNS phagocytes and neurons. *J Vis Exp*, doi:10.3791/51482 (2014).
54 Gustafsson, M. G. *et al.* Three-dimensional resolution doubling in wide-field fluorescence microscopy by structured illumination. *Biophys J* **94**, 4957-4970, doi:10.1529/biophysj.107.120345 (2008).
55 Hong, S., Wilton, D. K., Stevens, B. & Richardson, D. S. Structured Illumination Microscopy for the Investigation of Synaptic Structure and Function. *Methods Mol Biol* **1538**, 155-167, doi:10.1007/978-1-4939-6688-2_12 (2017).
56 Bolger, A. M., Lohse, M. & Usadel, B. Trimmomatic: a flexible trimmer for Illumina sequence data. *Bioinformatics* **30**, 2114-2120, doi:10.1093/bioinformatics/btu170 (2014).
57 Kim, D. *et al.* TopHat2: accurate alignment of transcriptomes in the presence of insertions, deletions and gene fusions. *Genome Biol* **14**, R36, doi:10.1186/gb-2013-14-4-r36 (2013).
58 Langmead, B., Trapnell, C., Pop, M. & Salzberg, S. L. Ultrafast and memory-efficient alignment of short DNA sequences to the human genome. *Genome Biol* **10**, R25, doi:10.1186/gb-2009-10-3-r25 (2009).
59 Trapnell, C. *et al.* Differential analysis of gene regulation at transcript resolution with RNA-seq. *Nat Biotechnol* **31**, 46-53, doi:10.1038/nbt.2450 (2013).

Supplementary Files

This is a list of supplementary files associated with this preprint. Click to download.

- supplementalfiguresC1qpaperNATCOMM.pdf